Communication

A MSM Visible-near-Infrared Wavelength Photodetector Based on PbS Quantum Dots/Porous Silicon Hybrid Structure

Yunlai He , Xuanzhang Li , Junyang Zhang , Zhendong Gao , Xinxin Li , Jiale Liu , Zhen Deng , Xiuyun Lei * , Chunhua Du , Yang Jiang , Haiqiang Jia , Wenxin Wang , Hong Chen

Posted Date: 15 September 2023

doi: 10.20944/preprints202309.1032.v1

Keywords: porous silicon; quantum dots; near-infrared

Brief Report

A MSM Visible-near-Infrared Wavelength Photodetector Based on PbS Quantum Dots/Porous Silicon Hybrid Structure

Yunlai He [1], Xuanzhang Li [2], Junyang Zhang [2], Zhendong Gao [2], Xinxin Li [2], Jiale Liu [2], Zhen Deng [2], Xiuyun Lei [1,*], Chunhua Du [2], Yang Jiang [2], Haiqiang Jia [2], Wenxin Wang [2] and Hong Chen [2]

[1] Key Laboratory of Nonferrous Materials and New Processing Technology, Ministry of Education, Guangxi Key Lab of Optical and Electronic Functional Materials and Devices, College of Materials Science and Engineering, Guilin University of Technology; Guilin, 541004, China; heyunlai96@163.com (Yunlai He)

[2] Key Laboratory for Renewable Energy, Beijing Key Laboratory for New Energy Materials and Devices, Beijing National Laboratory for Condensed Matter Physics, Institute of Physics, Chinese Academy of Sciences, Beijing 100190, China; lixuanzhang16@mails.ucas.ac.cn (Xuanzhang Li); zhangjunyang@iphy.ac.cn (Junyang Zhang); gaozhendong@iphy.ac.cn (Zhendong Gao); xinxin.li@iphy.ac.cn (Xinxin Li); 15661661060@163.com (Jiale Liu); zhen.deng@iphy.ac.cn (Zhen Deng.); duchunhua@iphy.ac.cn (Chunhua Du); jiangyang@iphy.ac.cn (Yang Jiang); mbe2@iphy.ac.cn (Haiqiang Jia); wxwang@iphy.ac.cn (Wenxin Wang); hchen@iphy.ac.cn (Hong Chen)

* Correspondence: xylei@glut.edu.cn

Abstract: porous silicon-based photodetectors have attracted more researches due to their high luminous efficiency, good stability and low cost. In this paper, a PbS quantum dots/porous silicon hybrid structure has been fabricated. The PbS quantum dots (QDs) partly infiltrated into the porous silicon (PSi) layer and partly deposited on its surface, which could increase the absorption of near-infrared wavelength range and extend the light absorption in silicon for wavelengths longer than 1100 nm. After that, A metal-semiconductor-metal (MSM) device is fabricated and its response spectrum could extend to the 1200 nm at -3 V. As a silicon-based photodetector (PD), one can envision its role for operation from visible light to short-wavelength infrared range.

Keywords: porous silicon; quantum dots; near-infrared

1. Introduction

As a silicon-based photodetector (PD), one can envision its role for operation from visible light to short-wavelength infrared range. Si-based Photodetectors, such as Complementary Metal Oxide Semiconductor (CMOS), have played a critical role in the daily life due to their advantages of low cost, high stability, high response speed, and high adaptability [1]. As the response wavelength increase from visible to near infrared range, the light collection efficiency becomes lower. To increase the absorption of near-infrared wavelength range and extend the light absorption in silicon for wavelengths longer than 1100nm, several approaches have been performed, such as metalens and microlens, which could offer good performance [2-5]. Recently, the porous silicon (PSi) template has attracted much attention due to its unique internal photoemission and filling property [6]. PSi is a mature material with low cost fabrication and its application has been expanded in recent years, such as GeSi template [7], biomarkers [8,9], solar cells [10,11] and light-emitting diodes [12,13]. PbS quantum dots (QDs) with ~3 nm diameter has a significant quantum effect, and its emission spectrum can cover the near-infrared band range. In addition, the PbS QDs has a good photoelectrical performance with high color purity, good stability and easy mass production [14], thus they have been utilized for biological and other detection [15]. Gaur et al. have investigated highly sensitive dual-mode labeled detection of biotin using reflection interference and fluorescence generated by conjugations of QDs-biotin and streptavidin probes immobilized on the PSi pore walls [16]. Bashkany

Preprints (www.preprints.org) | NOT PEER-REVIEWED | Posted: 15 September 2023 doi:10.20944/preprints202309.1032.v1

et al. used the microwave-assisted chemical bath deposition (MA-CBD) method to deposit PbS on the PSi prepared by photoelectric chemical etching [17]. Nayef et al. prepared Al/TiO2 nanoparticles/PSi structure ultraviolet (UV) photodetector by coating TiO2 nanoparticles (NPs) on PSi [18]. Ismail et al. prepared photodetectors with responses at 570nm and 700nm by infiltrating CdS NPs into PSi [19]. However, the above methods for preparing NPs/PSi structures require complicated fabrication and the electrical properties of the structures in the visible-near-infrared (Vis-NIR) wavelength are not well studied. In this paper, PbS QDs with an average particle size of ~3nm and an emission wavelength of 950nm were employed to form a PbS QDs/PSi template by a drop casting method compounded with the PSi obtained by electrochemical etching. Furthermore, A metal-semiconductor-metal (MSM) device is fabricated and its response spectrum could extend to the 1200 nm at -3 V. As a silicon-based photodetector (PD), one can envision its role for operation from visible light to short-wavelength infrared range.

2. Materials and Methods

Crystal silicon(c-Si) is purchased from Suzhou Yancai Micro-nano Technology. The chemical used in the experiment is analytically pure, which is purchased from Sinopharm Chemical. PbS QDs and toluene solvents are purchased from Xingshuo Nano.

PSi is prepared using electrochemical etching of (100) oriented boron doped p-type silicon wafer (p-Si) of thickness and resistivity 400 μm and (1-10) Ω · cm respectively. Prior to etching, the rectangular Si of $2 \times 3\ cm^2$ is cleaned by RCA process followed by soaking in dilute hydrofluoric acid (HF, >40%) to remove the native oxide and rinsing with de-ionized (DI) water. The electrolyte was a mixture of HF and ethyl alcohol (EtOH, >99.9%) with a volume ratio of 1: 2. We used a self-built electrochemical etching equipment with a Teflon tank that can be manually raised and lowered in height. The square area of $2 \times 2\ cm^2$ was soaked in electrolyte as anode and platinum piece as cathode. The morphology of PSi was controlled by changing current density and time, as shown in Table 1. The constant current source was provided by the Keithley 2400 source meter controlled by Lab-view 2006. Finally, PSi was rinsed in EtOH with low surface tension for 5min and dried with nitrogen to protect the integrity of it.

Table 1. Parameters of comparative experimental.

Name	Resistivity / Ω · cm	Orientation	HF:EtOH	t/min	J/mA · cm^{-2}
S11	1-10	<100>	1：2	10	5
S21	1-10	<100>	1：2	10	10
S31	1-10	<100>	1：2	10	20
S22	1-10	<100>	1：2	20	10
S23	1-10	<100>	1：2	40	10

Drop casting technique was employed to incorporating the PSi samples with PbS QDs [20,21]. Dropped 200 μl of 0.3 mg/ml PbS QDs dissolved in toluene on PSi using a pipette. The sample was placed at room temperature for 30 min until the toluene evaporated completely and QDs were physically coasted on the porous surface of PSi [22].

A 50 nm Al layer was evaporated at a rate of 1 A/s by electron beam evaporation system (FU-12PEB) on the S22 (10 mA/cm^2-20 min) covered with an interdigitated shadow mask of dimension $6 \times 6\ cm^2$ to form an Al/PbS QDs/PSi MSM configuration [23], as shown in Figure 1.

Preprints (www.preprints.org) | NOT PEER-REVIEWED | Posted: 15 September 2023 doi:10.20944/preprints202309.1032.v1

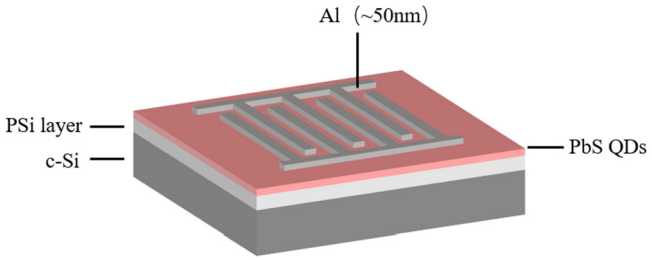

Figure 1. Schematic diagram of Al/QDs/PSi MSM structure.

The surface morphology of the prepared samples was completed by ultra-high resolution cold field emission scanning electron microscopy (HR-SEM, Regular 8100) and transmission electron microscopy (TEM, JEOL-2100 plus), operating voltages are 10 kV and 200 kV. TEM samples were prepared using a focused ion beam (FIB) dual beam system (Helios Nanolab 600i) with an operating voltage of 0.1-30kV. To explored the photoluminescence (PL) characteristics of the sample, a PL spectrometer (RMP BLUE) equipped with 226 nm and 532 nm lasers were employed. Ultraviolet-visible-near-infrared (UV-Vis-NIR) spectrum (Agilent, Cary 5000) was used to characterize the refractive index of the sample. I-V spectra of dark and illumination were measured by Keithley 4200 source meter, in which the test light source in illumination was provided by 905 nm laser (effective output power of 15 mW). Response spectra was achieved with a Fourier transform infrared (FT-IR) spectrometer (Bruker GmbH, Vertex-70v).

3. Results and discussion

Figure 2 shows the SEM cross-sectional image of PSi with and without PbS QDs, respectively. Dense, uniform and vertically sponge-like nano-structures with ~700 nm thickness formed on Si substrates are shown in Figure 2(a), which is mainly caused by the <100> crystal orientation of crystalline silicon [24]. QDs can be easily infiltrated into pores due to the hydrophobicity of the PSi structure and the weak surface tension of toluene. PSb QDs with a diameter of 3 nm can freely pass through the high-porosity layer with a pore size at least three times its size (9 nm) until be blocked by the low-porosity layer with the pore size reduced below 3 nm [25]. Figure 2(b) shows that a part of the PbS QDs remain on the surface of PSi, forming a layer of QDs with a relatively uniform thickness (~170 nm). This may be due to the small pores size of PSi that make some clusters gather on its surface. The 768nm PSi layer increases by 69nm compared to a single PSi, which is due to the less controlled electrochemical anode etching resulting in uneven etching. The supple skeleton of the PSi layer reduced the stress that was induced in the evaporation phase and limited the formation of cracks in the PbS layers [26].

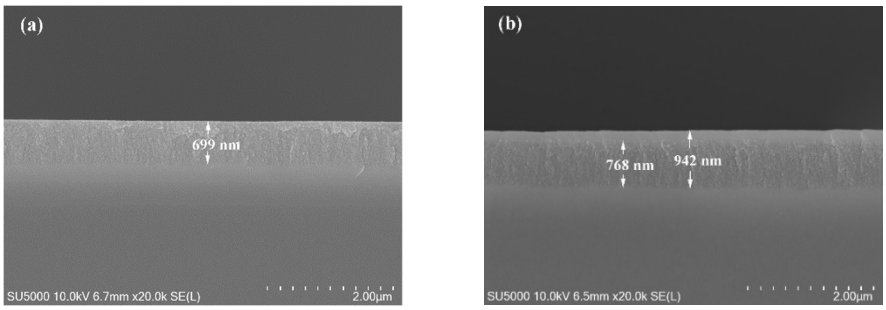

Figure 2. SEM of (a) PSi (10 mA/cm^2-20 min) and (b) PbS QDs/PSi (10 mA/cm^2-20 min) structure.

To determine the distribution of PbS QDs in the hybrid structure, energy dispersive spectroscopy (EDS) analysis of the cross-section is carried out, as shown in Figure 3. It can be clearly seen that there are Pb and S atoms in the PSi, which means that PbS QDs are successfully infiltrated into PSi. Meanwhile, the thin PbS layer on PSi surface indicates that a uniform surface layer of QDs is formed.

Preprints (www.preprints.org) | NOT PEER-REVIEWED | Posted: 15 September 2023 doi:10.20944/preprints202309.1032.v1

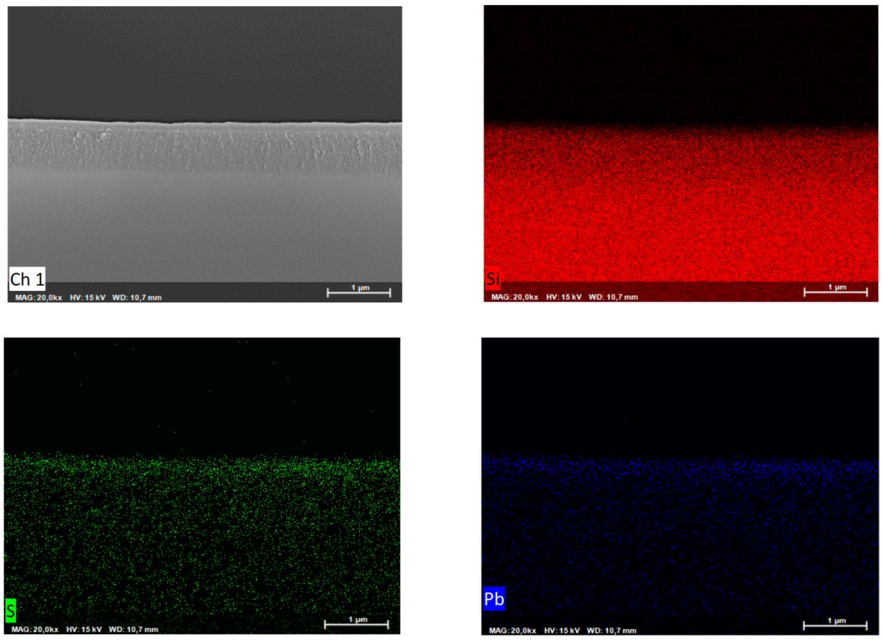

Figure 3. Cross-sectional EDS analysis of PbS QDs/PSi structure under SEM.

After that, TEM is employed to explore the microstructure of PbS QDs/PSi hybrid structure in detail. Figure 4(a) is a cross-sectional view of QDs/PSi, which shows that the thickness of PSi is ~847 nm and the PbS QDs on the surface is ~180 nm, which is consistent with the SEM results. Platinum (Pt) film can be found on the surface of the PbS QDs/PSi structure because Ga^+ in FIB has a certain beam width rather than a geometric straight line, which will damage the upper surface when cutting the sample. The high hardness properties of Pt can protect the upper surface. A 100 nm transition region is found at the interface of PbS and PSi. To explore the microscopic morphology of this region, a high-magnification TEM as shown in Figure 4(b) is performed. A layer of black spots is scattered near the interface of PbS QDs and PSi, which may be PbS QDs infiltrated into the pores of PSi.

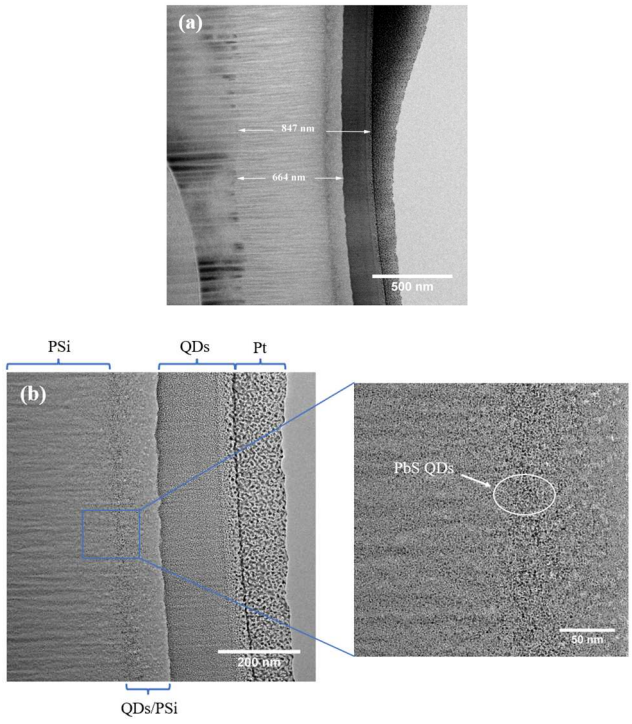

Figure 4. (a) Cross-sectional TEM and (b) local high-magnification TEM image of PbS QDs/PSi.

Preprints (www.preprints.org) | NOT PEER-REVIEWED | Posted: 15 September 2023 doi:10.20944/preprints202309.1032.v1

To explore the element distribution in the PbS QDs/PSi structure, dark field EDS of the hybrid region of PbS QDs and PSi is carried out. According to Figure 5, it can be concluded that PbS has partially penetrated into PSi, which is attributed to the brighter appearance of heavy particles (Pb) in the dark field mode. Through EDS analysis, it can demonstrate that a part of PbS is coated on the surface of PSi, and the other part infiltrates into the pores of PSi, which is consistent with our previous conjecture.

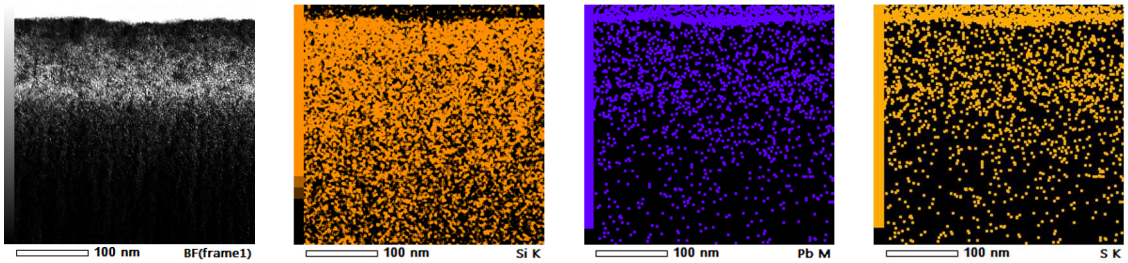

Figure 5. Dark-field EDS of PbS QDs/PSi interface region under TEM.

Optical properties of the PSi and PbS QDs studied through UV-Vis-NIR and PL spectra are recorded. Figure 6 compares the absolute UV-Vis-NIR (300-800 nm) reflectance spectra of c-Si and PSi. From the figure, it can be observed that c-Si exhibits 35-45% reflectivity, while PSi decreases reflectivity to 15-25%. These results indicates that absorption of PSi in the absolute spectral range is about 2 times higher than that of c-Si, which results from the porous structure with rough surface [27]. In addition, because the surface of PSi has more defects than that of c-Si, trap levels are formed at the band edge, which is easy for electron transmission and conducive to allowing more photons to input [28]. Figure 6(b) shows PL and Vis-NIR absorption spectra of PbS QDs, it can be seen that PbS QDs show onset and offset absorption band edge at ~950 nm and ~700 nm respectively in Vis-NIR region. As shown in Figure 6(b), PbS QDs has a strong PL peak appears in ~950 nm corresponding to absorption spectra, thereby it can be used as one of the candidates for near-infrared response of multi-wavelength detectors.

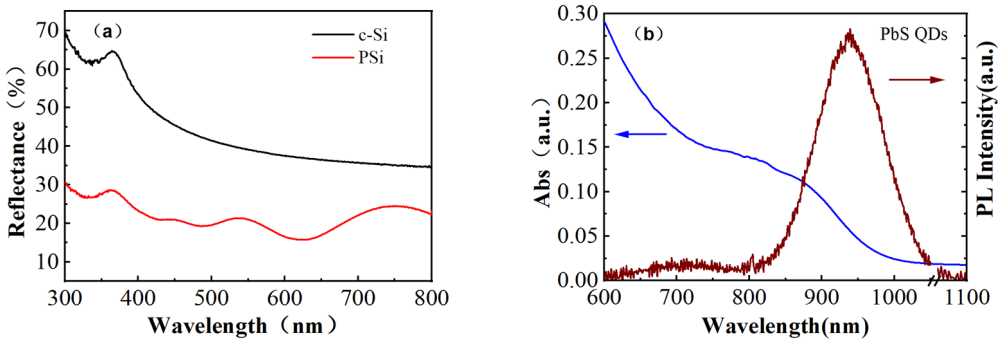

Figure 6. (a) UV-Vis-NIR absorption spectra of c-Si and PSi (10 mA/cm²-20 min). (b) PL and UV-Vis-NIR absorption spectra of PbS QDs.

Comparative experiments under different etching time and current density are set up to explore the effect of pore on PL of PSi. Figure 7 is the physical and schematic diagram taken during the PL test of S22 (10 mA/cm²-20 min) under the 266 nm laser. It can be clearly seen that the obtained PSi appears red under the laser. Figure 8(a) compares the PL of PSi under the etching time of 10 min, 20 min and 40 min respectively. Finally, an emission peak is appeared at ~700 nm, and PL shifts blue with the increase of etching time. Since the etching time mainly affects the depth of PSi, it can be considered that PL shifts blue with the increase of depth. The structure of the nano-PSi layer is actually a stack of nano-Si grains. The size of nano-grains gradually decreases with the increase of etching time, which makes the distance between them gradually increase and eventually manifested as an increase in depth. The PL of PSi is mainly due to the nano-Si grains in it. Therefore, according to the quantum confinement effect, the increase of etching time will cause the band gap widening

Preprints (www.preprints.org) | NOT PEER-REVIEWED | Posted: 15 September 2023 doi:10.20944/preprints202309.1032.v1

and PL blue shifting [29]. Figure 8(b) shows the PL of PSi at different current densities. We can find that the PL of PSi undergoes a blue shift as the current density increases. The current density mainly affects the pore size of PSi, so we can determine that PSi has a blue shift with the increase of pore size. With the increase of current density, the aggravation of etching results in a decrease in the size of Si nanoparticles and an increase in the distance between them, which leads to the PL blue shift of PSi [30]. The change of current density on pores is mainly manifested in pore size, which is different from that of etching time which mainly affects pore depth. In general, PL peak of PSi will have a blue shift with the increase of pore size and depth. From Figure 8(a) and (b), a PL emission peak of PSi is found at ~700 nm, which is not available in c-Si. It proves that PSi has changed from an indirect bandgap to a direct bandgap compared with c-Si [31]. This is attribute to the quantum confinement effect of the nano-Si grains inside the porous silicon and the Si-H dangling bonds attached to the surface of the pores resulting in defect energy levels at the edge of the Si bandgap and widening the bandgap. The PL of PbS QDs/PSi is shown in Figure 8(c), it exhibits two emission peaks at ~650 nm and ~925 nm corresponding to PSi and PbS QDs respectively, which proves that QDs successfully recombine with PSi to form a heterojunction [32,33]. The pore size can be controlled by adjusting the experimental conditions to adjust the PL emission band, and compound with the PL band of QDs [34].

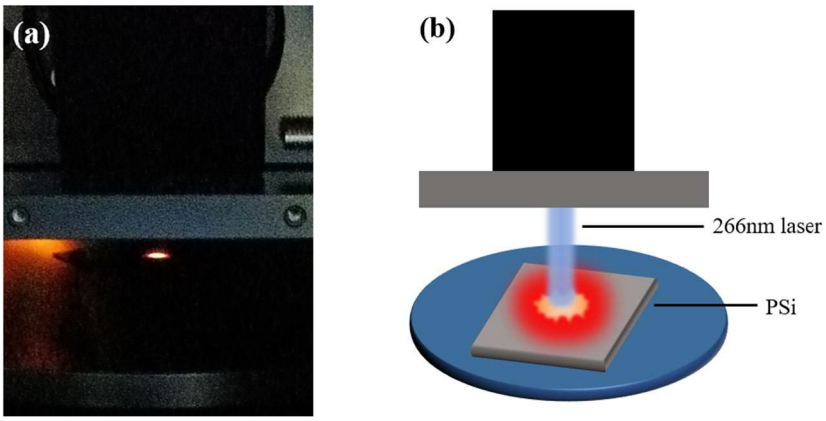

Figure 7. (a) Physical and (b) schematic diagram of PL characterization.

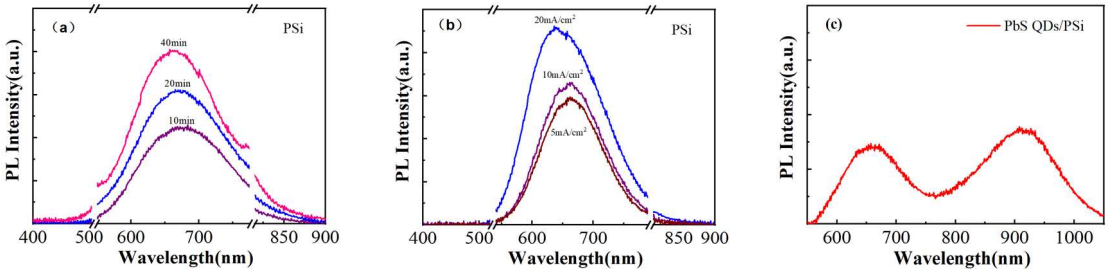

Figure 8. PL of PSi under (a) different etching times and (b) different current densities. (c) PL of PbS QDs/PSi (10 mA/cm²-20 min).

To analyse electrical properties of the prepared Al/PbS QDs/PSi MSM configuration, current-voltage (I-V) characteristics under dark and 905nm laser in the applied bias range of -5 V to 5 V and responsivity characteristics in the applied bias of -3 V are recorded for MSM electrode configuration. As can be seen from Figure 9(a), I-V spectra shows almost symmetric enhancement of rectification in both forward and reverse bias condition with a photocurrent to dark-current ratio of 3.07 and 1.10 at ±3 V respectively. There is no zero-point shift phenomenon of self-powered detector which is in agreement with the symmetry of MSM device, and indicates that etching of PSi is relatively uniform [35]. The dark current of Al/QDs/PSi configuration is ~5×10-7 A, which shows that it has a weak dark current. It generates a current of ~1×10-6 A under the irradiation of 905 nm laser, and the symmetry of its I-V curve remains good, which further shows that the device has excellent stability under illumination. The small particle size characteristics of PbS QDs also contribute to the photocurrent,

due to the fact that for larger clusters, the band arrangement at the PbS QDs/PSi interface is not conducive to carrier transfer [36]. The response spectra of MSM configuration is shown in Figure 9(b), it can be observed that there is a certain optical response at 850 nm and 1150 nm, which may correspond to a combination of PSi, PbS QDs, and c-Si substrates [37]. In brief, Vis-NIR wavelength detectors of PSi have been successfully prepared, while its corresponding light intensity is weak, which may be attribute to the low uniformity of PSb QDs infiltrated into PSi and the oxidation layer between the Al electrode and the PSi [38,39].

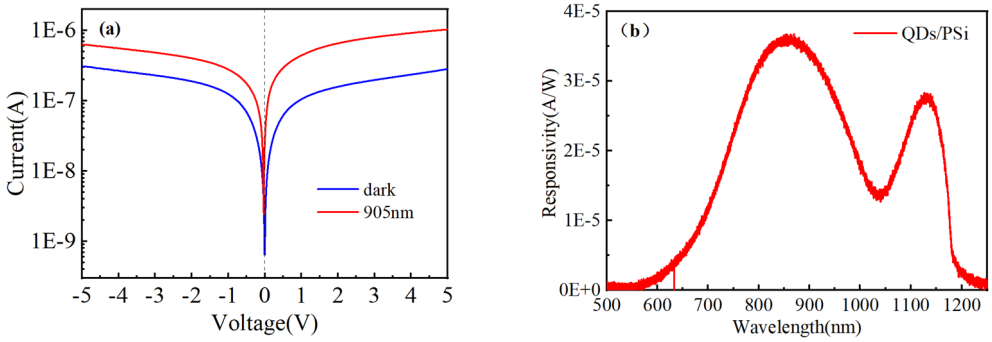

Figure 9. (a) Light/dark IV spectra of QDs/PSi (10 mA/cm²-20 min). (b) Photo-response spectra of QDs/PSi under 905 nm laser at -3 V.

4. Conclusions

In conclusion, we have successfully fabricated the PbS/PSi hybrid structure and thus a MSM device for Vis-NIR detector is demonstrated. The experimental results indicate that part of the PbS QDs were infiltrated into PSi to a depth of ~100 nm, while other parts were clustered on the surface. The response spectra shows that there are two response peaks at~850 nm and~1150 nm in the visible and near-infrared region. This work could provide a valuable reference for the future research of PSi application in the field of infrared detection.

Author Contributions: Conceptualization, Yunlai He, Xuanzhang Li, Junyang Zhang, Zhendong Gao, Xinxin Li, Jiale Liu, Zhen Deng, Xiuyun Lei, Chunhua Du, Yang Jiang, Haiqiang Jia, Wenxin Wang, Hong Chen; Methodology, Yunlai He, Xuanzhang Li, Junyang Zhang, Zhendong Gao, Xinxin Li, Jiale Liu, Zhen Deng, Xiuyun Lei, Chunhua Du, Yang Jiang, Haiqiang Jia, Wenxin Wang and Hong Chen; resources, Zhen Deng, Xiuyun Lei, Chunhua Du, Yang Jiang, Haiqiang Jia, Wenxin Wang and Hong Chen; Data curation, Yunlai He, Xiuyun Lei and Zhen Deng; Writing—original draft preparation, Yunlai He; Writing-review and editing, Yunlai He, Zhen Deng and Xiuyun Lei. All authors have read and agreed to the published version of the manuscript. All authors have read and agreed to the published version of the manuscript.

Acknowledgments: In this section, you can acknowledge any support given which is not covered by the author contribution or funding sections. This may include administrative and technical support, or donations in kind (e.g., materials used for experiments). We appreciate the financial support from the Center for Clean Energy and Huairou Division, Institute of Physics, Chinese Academy of Sciences.

Conflicts of Interest: The authors declare no conflict of interest

References

1. Bao, S.; Wang, Y.; Lina, K.; Zhang, L.; Wang, B.; Sasangka, W.A.; Lee, K.E.K.; Chua, S.J.; Michel, J.; Fitzgerald, E.; et al. A Review of Silicon-Based Wafer Bonding Processes, an Approach to Realize the Monolithic Integration of Si-CMOS and III-V-on-Si Wafers. *J. Semicond.* **2021**, *42*, doi:10.1088/1674-4926/42/2/023106.
2. Deng, Z.; Yang, Q.; Chen, F.; Meng, X.; Bian, H.; Yong, J.; Shan, C.; Hou, X. Fabrication of Large-Area Concave Microlens Array on Silicon by Femtosecond Laser Micromachining. *Opt. Lett.* **2015**, *40*, 1928, doi:10.1364/ol.40.001928.
3. Afridi, A.; Canet-Ferrer, J.; Philippet, L.; Osmond, J.; Berto, P.; Quidant, R. Electrically Driven Varifocal Silicon Metalens. *ACS Photonics* **2018**, *5*, 4497–4503, doi:10.1021/acsphotonics.8b00948.

4. Chantakit, T.; Schlickriede, C.; Sain, B.; Meyer, F.; Weiss, T.; Chattham, N.; Zentgraf, T. All-Dielectric Silicon Metalens for Two-Dimensional Particle Manipulation in Optical Tweezers. *Photonics Res.* **2020**, *8*, 1435, doi:10.1364/prj.389200.
5. Chang, Y.-C.; Chul Shin, M.; Phare, C.T.; Miller, S.A.; Shim, E.; Lipson, M. 2D Beam Steerer Based on Metalens on Silicon Photonics. *Opt. Express* **2021**, *29*, 854, doi:10.1364/oe.409711.
6. De La Mora, M.B.; Bornacelli, J.; Nava, R.; Zanella, R.; Reyes-Esqueda, J.A. Porous Silicon Photoluminescence Modification by Colloidal Gold Nanoparticles: Plasmonic, Surface and Porosity Roles. *J. Lumin.* **2014**, *146*, 247–255, doi:10.1016/j.jlumin.2013.09.053.
7. Wang, S.; Deng, Z.; Li, X.; Li, J.; Li, Y.; Xu, R.; Jiang, Y.; Ma, Z.; Wang, L.; Du, C.; et al. Fabrication, Structural and Optical Properties of a Virtual GeSi Template by Ge Filling the Porous Si Prepared by EC Etching. *Jpn. J. Appl. Phys.* **2020**, *59*, doi:10.35848/1347-4065/ab86ff.
8. Myndrul, V.; Viter, R.; Savchuk, M.; Koval, M.; Starodub, N.; Silamiķelis, V.; Smyntyna, V.; Ramanavicius, A.; Iatsunskyi, I. Gold Coated Porous Silicon Nanocomposite as a Substrate for Photoluminescence-Based Immunosensor Suitable for the Determination of Aflatoxin B1. *Talanta* **2017**, *175*, 297–304, doi:10.1016/j.talanta.2017.07.054.
9. Balderas-Valadez, R.F.; Agarwal, V.; Pacholski, C. Fabrication of Porous Silicon-Based Optical Sensors Using Metal-Assisted Chemical Etching. *RSC Adv.* **2016**, *6*, 21430–21434, doi:10.1039/c5ra26816h.
10. Omar, K.; Salman, K.A. Effects of Electrochemical Etching Time on the Performance of Porous Silicon Solar Cells on Crystalline N-Type (100) and (111). *J. Nano Res.* **2017**, *46*, 45–56, doi:10.4028/www.scientific.net/JNanoR.46.45.
11. Badawy, W.A. A Review on Solar Cells from Si-Single Crystals to Porous Materials and Quantum Dots. *J. Adv. Res.* **2015**, *6*, 123–132, doi:10.1016/j.jare.2013.10.001.
12. Kanaujia, P.K.; Singh, A.; Vijaya Prakash, G. Silicon-Based Inorganic–Organic Hybrid Nanocomposites for Optoelectronic Applications. *Energy Technol.* **2017**, *5*, 1795–1799, doi:10.1002/ente.201700355.
13. Shrivastava, M.; Kumari, R.; Parra, M.R.; Pandey, P.; Siddiqui, H.; Haque, F.Z. Electrochemical Synthesis of MoS2 Quantum Dots Embedded Nanostructured Porous Silicon with Enhanced Electroluminescence Property. *Opt. Mater. (Amst).* **2017**, *73*, 763–771, doi:10.1016/j.optmat.2017.09.029.
14. Dovzhenko, D.; Krivenkov, V.; Kriukova, I.; Samokhvalov, P.; Karaulov, A.; Nabiev, I. Enhanced Spontaneous Emission from Two-Photon-Pumped Quantum Dots in a Porous Silicon Microcavity. *Opt. Lett.* **2020**, *45*, 5364–5367, doi:10.1364/ol.400300.
15. Zhou, R.; Jia, Z.; Lv, X.; Huang, X. The Enhanced Sensitivity of a Porous Silicon Microcavity Biosensor Based on an Angular Spectrum Using CdSe/ZnS Quantum Dots. *Sensors* **2019**, *19*, 4872, doi:10.1109/JSEN.2021.3059878.
16. Gaur, G.; Koktysh, D.S.; Weiss, S.M. Immobilization of Quantum Dots in Nanostructured Porous Silicon Films: Characterizations and Signal Amplification for Dual-Mode Optical Biosensing. *Adv. Funct. Mater.* **2013**, *23*, 3604–3614, doi:10.1002/adfm.201202697.
17. Bashkany, Z.A.; Abbas, I.K.; Mahdi, M.A.; Al-Taay, H.F.; Jennings, P. A Self-Powered Heterojunction Photodetector Based on a PbS Nanostructure Grown on Porous Silicon Substrate. *Silicon* **2018**, *10*, 403–411, doi:10.1007/s12633-016-9462-4.
18. Nayef, U.M.; Hubeatir, K.A.; Abdulkareem, Z.J. Ultraviolet Photodetector Based on TiO2 Nanoparticles/Porous Silicon Hetrojunction. *Optik (Stuttg).* **2016**, *127*, 2806–2810, doi:10.1016/j.ijleo.2015.12.002.
19. Ismail, R.A.; Khashan, K.S.; Alwan, A.M. Study of the Effect of Incorporation of CdS Nanoparticles on the Porous Silicon Photodetector. *Silicon (2.670/Q4)* **2017**, *9*, 321–326, doi:10.1007/s12633-016-9446-4.
20. Kriukova, I.; Samokhvalov, P.; Nabiev, I. Near-Infrared Photoluminescent Hybrid Structures Based on Freestanding Porous Silicon Photonic Crystals and PbS Quantum Dots. *Appl. Nanosci.* **2022**, *12*, 3315–3320, doi:10.1007/s13204-021-02055-4.
21. Nayef, U.M.; Kamel, R.I. Enhancement the Electrical Properties of Porous Silicon for Photo-Detectors Applications by Depositing Bi2O3 Nanoparticles. *Optik (Stuttg).* **2020**, *207*, 163847, doi:10.1016/j.ijleo.2019.163847.
22. Chandrasekaran, S.; Macdonald, T.J.; Mange, Y.J.; Voelcker, N.H.; Nann, T. A Quantum Dot Sensitized Catalytic Porous Silicon Photocathode. *J. Mater. Chem. A* **2014**, *2*, 9478–9481, doi:10.1039/c4ta01677g.

23. Das, M.; Sarmah, S.; Sarkar, D. Photo Sensing Property of Nanostructured CdS-Porous Silicon (PS):P-Si Based MSM Hetero-Structure. *J. Mater. Sci. Mater. Electron.* **2019**, *30*, 11239–11249, doi:10.1007/s10854-019-01470-2.
24. Tokranova, N.A.; Novak, S.W.; Castracane, J.; Levitsky, I.A. Deep Infiltration of Emissive Polymers into Mesoporous Silicon Microcavities: Nanoscale Confinement and Advanced Vapor Sensing. *J. Phys. Chem. C* **2013**, *117*, 22667–22676, doi:10.1021/jp405071n.
25. Qiao, H.; Guan, B.; Böcking, T.; Gal, M.; Gooding, J.J.; Reece, P.J. Optical Properties of II-VI Colloidal Quantum Dot Doped Porous Silicon Microcavities. *Appl. Phys. Lett.* **2010**, *96*, 161106, doi:10.1063/1.3404183.
26. Amirhoseiny, M.; Hassan, Z.; Ng, S.S. Fabrication of InN Based Photodetector Using Porous Silicon Buffer Layer. *Surf. Eng.* **2013**, *29*, 772–777, doi:10.1179/1743294413Y.0000000189.
27. Das, M.; Sarmah, S.; Barman, D.; Sarma, B.K.; Sarkar, D. Distinct Band UV–Visible Photo Sensing Property of ZnO-Porous Silicon (PS):P-Si Hybrid MSM Heterostructure. *Mater. Sci. Semicond. Process.* **2020**, *118*, 105188, doi:10.1016/j.mssp.2020.105188.
28. Sarkar, A.; Mukherjee, S.; Das, A.K.; Ray, S.K. Photoresponse Characteristics of MoS2 QDs/Si Nanocone Heterojunctions Utilizing Geometry Controlled Light Trapping Mechanism in Black Si. *Nanotechnology* **2019**, *30*, 485202, doi:10.1088/1361-6528/ab3c9f.
29. Başak, F.K.; Kayahan, E. White, Blue and Cyan Luminescence from Thermally Oxidized Porous Silicon Coated by Green Synthesized Carbon Nanostructures. *Opt. Mater. (Amst).* **2022**, *124*, 111990, doi:10.1016/j.optmat.2022.111990.
30. Gaur, G.; Koktysh, D.S.; Fleetwood, D.M.; Weller, R.A.; Reed, R.A.; Weiss, S.M. Influence of Interfacial Oxide on the Optical Properties of Single Layer CdTe/CdS Quantum Dots in Porous Silicon Scaffolds. *Appl. Phys. Lett.* **2015**, *107*, 063106, doi:10.1063/1.4928663.
31. Kim, D.H.; Lee, W.; Myoung, J.M. Flexible Multi-Wavelength Photodetector Based on Porous Silicon Nanowires. *Nanoscale* **2018**, *10*, 17705–17711, doi:10.1039/c8nr05096a.
32. Dhyani, V.; Dwivedi, P.; Dhanekar, S.; Das, S. High Performance Broadband Photodetector Based on MoS2/Porous Silicon Heterojunction. *Appl. Phys. Lett.* **2017**, *111*, 1–6, doi:10.1063/1.5004025.
33. Sun, L.; He, H.; Liu, C.; Lu, Y.; Ye, Z. Controllable Growth and Optical Properties of ZnO Nanostructures on Si Nanowire Arrays. *CrystEngComm* **2011**, *13*, 2439–2444, doi:10.1039/c0ce00844c.
34. Dovzhenko, D.; Martynov, I.; Samokhvalov, P.; Osipov, E.; Lednev, M.; Chistyakov, A.; Karaulov, A.; Nabiev, I. Enhancement of Spontaneous Emission of Semiconductor Quantum Dots inside One-Dimensional Porous Silicon Photonic Crystals. *Opt. Express* **2020**, *28*, 22705–22717, doi:10.1364/oe.401197.
35. Benyahia, K.; Djeffal, F.; Ferhati, H.; Bendjerad, A.; Benhaya, A.; Saidi, A. Self-Powered Photodetector with Improved and Broadband Multispectral Photoresponsivity Based on ZnO-ZnS Composite. *J. Alloys Compd.* **2021**, *859*, 158242, doi:10.1016/j.jallcom.2020.158242.
36. Hoyer, P.; Könenkamp, R. Photoconduction in Porous TiO2 Sensitized by PbS Quantum Dots. *Appl. Phys. Lett.* **1995**, 349, doi:10.1063/1.114209.
37. Ismail, R.A.; Kadhim, R.G.; Abdulridha, W.M. Effect of Multiwalled Carbon Nanotubes Incorporation on the Performance of Porous Silicon Photodetector. *Optik (Stuttg).* **2016**, *127*, 8144–8152, doi:10.1016/j.ijleo.2016.06.018.
38. Chou, C.M.; Cho, H.T.; Hsiao, V.K.S.; Yong, K.T.; Law, W.C. Quantum Dot-Doped Porous Silicon Metal Semiconductor Metal Photodetector. *Nanoscale Res. Lett.* **2012**, *7*, 291, doi:10.1186/1556-276X-7-291.
39. Das, M.; Sarmah, S.; Sarkar, D. UV-Visible Optical Photo-Detection from Porous Silicon (PS) MSM Device. *Superlattices Microstruct.* **2017**, *101*, 228–235, doi:10.1016/j.spmi.2016.11.052